Applied Catalysis B: Environmental 84 (2008) 185–195

Contents lists available at ScienceDirect

Applied Catalysis B: Environmental

journal homepage: www.elsevier.com/locate/apcatb

The highly active catalysts of nanometric CeO_2-supported cobalt oxides for soot combustion

Jian Liu [a], Zhen Zhao [a,*], Jiqiu Wang [a], Chunming Xu [a], Aijun Duan [a], Guiyuan Jiang [a], Qing Yang [b]

[a] State Key Laboratory of Heavy Oil Processing, China University of Petroleum, Beijing 102249, PR China
[b] Hefei National Laboratory for Physical Sciences at Microscale, University of Science and Technology of China, Hefei, Anhui Province 230026, PR China

ARTICLE INFO

Article history:
Received 31 January 2008
Received in revised form 23 March 2008
Accepted 30 March 2008
Available online 7 April 2008

Keywords:
Nanometric CeO_2-supported cobalt oxides
Catalysts
Soot combustion
Ceria
Cobalt

ABSTRACT

Nanometric CeO_2-supported cobalt oxide materials with variable Co/Ce atomic ratios were prepared by the method of ultrasonic-assisted incipient-wetness impregnation. The catalytic behaviors of a series of CoO_x/nmCeO_2 catalysts have been studied for soot combustion. XRD, XPS, Raman, UV–vis DRS and FT-IR spectroscopy characterization results indicated that CoO or cobalt–cerium solid solutions were formed in the samples with the low Co loading amount, while Co_3O_4 was formed in the samples with high Co loading amount. CoO_x/nmCeO_2 catalysts can further promote soot combustion in contrast to nanometric CeO_2. This improvement is related to the increase in the redox properties of the catalysts brought about by loading cobalt oxide on nanometric CeO_2. The TPR experiment results under hydrogen atmosphere indicated that the presence of Co decreases the reduction temperature of catalyst from 555 °C (nanometric CeO_2) to 286 °C (Co_{20}/nmCeO_2). On the other hand, attributing to nanoparticle effect and NO_2 formation, Co_m/nmCeO_2 oxide catalysts prepared in this study have very high activity for soot combustion. The best catalytic activity was obtained over Co_{20}/nmCeO_2 catalyst that T_{10}, T_{50}, T_{90} were 286 °C, 368 °C, 418 °C, respectively, and $S^m_{CO_2}$ was 98.8%. Compared with the blank case (i.e., without catalyst) for soot combustion, T_{50} decreased by more than 200 °C and $S^m_{CO_2}$ increased by 40% point. And this catalytic activity for the combustion of soot particle is as good as supported Pt catalysts, which is the best catalyst system so far reported for soot combustion under loose contact conditions. This temperature of soot combustion can ensure immediate activation of the catalyst on the filter under the conditions of diesel engine emissions.

1. Introduction

Diesel exhaust gases had traditionally been considered clean in comparison with the exhaust gases of gasoline vehicles, but the successful introduction of three-way catalyst (TWC) for use in gasoline-powered vehicles and the development of modern engines have changed this benefit of diesel engines. The particulate matter (mainly soot) emitted from diesel engines is one of the most serious pollutants in urban areas, but a catalytic device like TWC is not available for soot elimination. Thus, the search for soot reduction techniques is an issue of current scientific and technological research. The removal of soot particulate involves trapping it within a ceramic monolith and subsequently oxidizing it using O_2 and/or NO/O_2 mixtures to form CO_2 and CO. Exhaust gases of the typical diesel vehicle have a temperature ranging from 150 °C to 400 °C. As the soot combustion temperature is much higher than the operational temperature found in the exhaust pipe, the particulate matter combustion temperature should be lowered and consequently active catalysts must be developed in such temperature levels [1,2]. Teraoka et al. [3,4] firstly and systematically studied the catalytically simultaneous removal of soot and NO_x in oxygen-rich model exhaust. They reported that perovskite or spinel oxides were effective catalysts for soot combustion, whereby potassium acted as promoters. Hong et al. [5] reported that the partial substitution of Cs into A-site enhanced the catalytic activities of perovskite oxides for soot oxidation. These pioneering investigations reported the relevant catalytic activities under tight contact conditions between catalysts and soot particles, however, it is a loose contact between the catalysts on the surface of filter and soot particles under practical conditions [6,7]. Thus, it is very urgent to study and design the active catalysts for soot particulate oxidation under loose contact conditions.

* Corresponding author. Tel.: +86 10 89731586; fax: +86 10 69724721.
E-mail address: zhenzhao@cup.edu.cn (Z. Zhao).

0926-3373/$ – see front matter © 2008 Elsevier B.V. All rights reserved.
doi:10.1016/j.apcatb.2008.03.017

Neeft et al. [8] found a correlation between melting temperature of catalyst and its catalytic activity for soot loose contact with catalyst particle. They successfully developed a series of Cu-K-V-Cl and Cu-K-Mo-Cl catalysts which had low melting points and high catalytic activities for soot combustion. But these catalysts were easy to vaporize and cause new pollution for environment. In recent years, Oi-Uchisawa et al. [9,10] and Hinot et al. [11] studied the combustion of soot over supported noble metal Pt catalysts using NO/O_2 mixtures as oxidizing agents. The use of NO/O_2 as oxidizing agents promotes soot combustion over these materials through the operation of a NO_2 intermediate in the reaction mechanism. The supported-Pt catalysts exhibited a high level of catalytic activity to promote soot oxidation. This catalyst system is the best one so far reported for soot combustion under loose contact conditions. However, Pt is expensive and scarce. Therefore, it is significantly important to develop the cheap catalysts for soot combustion under loose contact conditions. As in the most of heterogeneous catalysis projects, the search of noble metal free diesel soot oxidation catalysts is a key object. Soot oxidations over cheap-metal oxides have been extensively studied and reviewed. Recent publications describe soot oxidation over PbO_x/CoO_x [12], supported- and mixed-vanadium oxides [13,14], and perovskite complex oxides [15]. If the cheap metal oxide catalysts might oxidize NO to NO_2 like Pt catalyst they could subtly change solid (soot)–solid (catalyst) contact into solid (soot)–gas (NO_2)–solid (catalyst) contact. Then, the catalyst should have good activity for oxidizing soot to CO_2 and CO under loose contact conditions.

Cerium oxides and cobalt oxides can play an important role in oxidation reaction. CeO_2 is an important component in the TWC [16,17]. The main properties of cerium oxides for this TWC application are (i) a large oxygen storage capacity via the redox process $Ce^{4+} \leftrightarrow Ce^{3+}$; (ii) improvement of the dispersion of noble metals; (iii) improvement of the thermal stability of supports; and (iv) promotion of the water–gas shift reaction. Cobalt-based oxides are the good candidate catalysts for diesel soot combustion. Co_3O_4 shows highly catalytic activity for the combustion of CO and organic compounds. The activity and selectivity of such catalysts are related to the strong redox ability of CoO_x [18]. Despite the fact that CeO_2 and Co_3O_4 catalysts have been extensively studied for oxidation reaction and TWC application, few detailed studies have analyzed the utilization of CeO_2-supported cobalt oxide materials for soot combustion. Harrison et al. [19] exploringly reported the CoO/CeO_2 catalytic system for soot oxidation. However, they investigated on the CoO/CeO_2 catalysts for soot oxidation under tight contact conditions, and the promotion role of NO_x in the reaction atmosphere for soot combustion was not well illustrated. Furthermore, applications of catalyst materials depend on their sizes and morphology. It is well known that nanoparticles usually have specific shape and higher surface energy, which leads to very high activity in some catalytic reactions. Thus, nanometer oxide materials have become a new study focus because of their potential application in catalysis [20,21]. Because of these reasons, new nanometer CeO_2-supported CoO_x catalysts were prepared and their catalytic performances for diesel soot combustion under the loose contact between soot and catalysts were investigated in this work. And a similar mechanism as Pt catalyst oxidized NO to NO_2 is found for soot combustion over the nanometer CeO_2-supported CoO_x catalysts.

2. Experimental

2.1. Catalyst preparation

Co_3O_4 and nanometric CeO_2 powder were prepared by the auto-combustion method assisted by rotating evaporation. The $Co(NO_3)_2$ or $Ce(NO_3)_3$ were used as starting materials. A solution of citric acid 100% in excess was chosen as a ligand. The resulting solution was heated by a rotating evaporator at 50 °C in water bath under $P = 0.02$ MPa vacuum. After about eighty percent of water was evaporated, the mixing solution was heated at a flow air atmosphere by an electric furnace with 2 kW power and evaporated to dryness with vigorous stirring, following burning and giving off a great amount of gases, and finally the precursor was calcined at 600 °C for 4 h in a static air.

Nanometric CeO_2-supported cobalt oxide catalysts were prepared by the method of ultrasonic-assisted incipient-wetness impregnation. The nitrate of Co was used as starting materials with appropriate stoichiometry. The catalysts will be generically named as $Co_m/nmCeO_2$, where m is the molar ratio of 100 Co/Ce ($m = 0.1$, 1, 4, 10, 20, 50, 100).

2.2. Catalytic activity measurement

The catalytic oxidation activities of the prepared samples were evaluated with a temperature-programmed oxidation reaction (TPO) on a fixed-bed tubular quartz system. The reaction temperature was controlled through a PID-regulation system based on the measurements of a K-type thermocouple and varied from 200 °C to 700 °C at a 2 °C/min rate during each TPO run. The model soot, Printex-U, used in this work was provided by Degussa. Its primary particle size was 25 nm and specific surface was 100 m^2/g. Catalyst and soot were mixed at a mass ratio of 10:1 with a spatula in order to reproduce the loose contact mode, which is the most representative model of diesel particles flowing through a catalytic filter [6–10]. 100 mg of the mixture placed in the tubular quartz reactor (reactor diameter $\phi = 8$ mm). The occurrence of heat and mass transfer limitations would influence the observed reaction rates. In addition, it was also found to affect soot combustion temperatures about 0–5 °C. In order to accurately detect the true reaction temperatures, the catalyst-soot fixed bed was sandwiched between two quartz-wool layers. And the tip of a K-type thermocouple was located well inside the catalyst bed itself. The reaction temperature was controlled through a PID-regulation system based on the measurements of an external K-type thermocouple. Reactant gases containing 5% O_2 and 2000 ppm NO balanced with He were passed through a mixture of the catalyst and soot at a flow rate of 50 ml/min (STP). The outlet gas composition from the reactor passed through a 1 cm^3 sampling loop of a six-point gas-sampling valve before it was being injected into an on-line gas chromatograph (GC). The GC with both a thermal conductivity detector (TCD) and a flame ionization detector (FID) was used to analyze the gaseous mixture. The TCD was used to measure the concentration of O_2, N_2, CO after separating these gases over a molecular sieve 5A column. The FID was employed to determine CO and CO_2 concentrations after separating these gases over a Porapak N column and converting them to methane over a Ni catalyst at 380 °C. The selectivity to CO_2 formation (S_{CO_2}) was defined as that the CO_2 outlet concentration (C_{CO_2}) divided by the sum of the CO_2 and CO outlet concentrations, i.e., $S_{CO_2} = C_{CO_2}/(C_{CO} + C_{CO_2})$. $S^m_{CO_2}$ was denoted as the S_{CO_2} at the maximum temperature at which soot-burnt rate was the highest. The catalytic activity was evaluated by the values of T_{10}, T_{50}, and T_{90}, which were defined as the temperatures at which 10%, 50%, and 90% of the soot, respectively, were oxidized during the TPO procedure.

In order to investigate the effect of NO_2 on the soot combustion, NO oxidation experiments were carried out by the means of TPO and NO_2 concentrations were detected by Quantachrome autosorb-1C mass spectroscope. The blank soot (without catalyst) and two typical catalysts ($nmCeO_2$ and $Co_{20}/nmCeO_2$) were used for activity evaluation. The other experimental condition is the same as soot combustion in TPO reaction.

2.3. Catalyst characterization

The crystal structures of the fresh catalysts were determined by a powder X-ray diffractometer (Shimadzu XRD 6000), using Cu Kα (λ = 0.1542 nm) radiation combined with Nickel filter operating at 40 kV and 10 mA. The diffractometer data were recorded for 2θ values between 15° and 80° at a scanning rate of 4°/min. The patterns were compared with JCPDS reference data for phase identification. The Scherrer equation was used to calculate the crystal size of the studied samples. The surface morphology of the samples was observed by SEM (S-4800, Hitachi company, Japan). XPS spectra were recorded using a PerkinElmer PHI 5600 Ci spectrometer with a standard Al Kα source (1486.6 eV) working at 350 W. The working pressure was less than 1×10^{-8} Pa. The spectrometer was calibrated by assuming the binding energy (BE) of the Au $4f_{7/2}$ line to lie at 84.0 eV with respect to the Femi level. The standard deviation in the BE values of the XPS line is 0.10 eV. The BET specific surface areas were measured with linear parts of the BET plot of the N_2 isotherms, using a Micromeritics ASAP 2010 analyzer. Raman spectra were performed on LabRAM HR spectrometer manufactured by Horiba Jobin Yvon company, France. The laser excitation wavelength was 514 nm. The UV–vis NIR DRS experiments were performed on Hitachi U-4100 UV–vis spectrophotometer with the integration sphere diffuse reflectance attachment. The powder samples were loaded in a transparent quartz cell and were measured in the region of 200–800 nm at room temperature. The standard nanometric CeO_2 support reflectance was used as the baseline for the corresponding catalyst measurement.

FT-IR absorbance spectra were obtained in the wave number ranging between 6000 cm^{-1} and 400 cm^{-1} via an FTS-3000 spectrophotometer manufactured by American Digilab company. For the transmission IR experiments under ambient conditions, the measured wafer was prepared as KBr pellet with the weight ratio of sample to KBr, 1/100. The resolution was set at 2 cm^{-1} during measurement. For in situ diffuse reflection infrared Fourier transformed (DRIFT) experiments, it did not need to use KBr as diluent. The spectra were recorded in the range of 400–4000 cm^{-1} after 256 scans at a resolutiom of 4 cm^{-1}. The powder sample was placed in a sample holder assembly in a Harrick Praying Mantis DRIFT cell. The gases were supplied by individual mass flow controllers with a total flow rate of 50 ml/min. Before reactant gases entering, the sample was pretreated with 5% O_2 in helium at 300 °C for 30 min. The sample was then cooled to reaction temperature and equilibrated in a helium atmosphere. After the sample had cooled to the reaction temperature, a spectrum of the treated sample was taken as the background at that temperature. The in situ experiment was performed by the introduction of 2000 ppm NO and 5% O_2 in helium. Meanwhile, the IR spectra were sequentially recorded at the different reaction temperatures of 100 °C, 200 °C, 300 °C, 350 °C, 400 °C, 450 °C, and 500 °C, respectively.

NO adsorption on $Co_{20}/nmCeO_2$ catalyst was carried out in the quartz flow reactor using 200 mg sample. The catalyst was pretreated in a gas flow of O_2/He (10% O_2 by volume) at 500 °C for 1 h and then cooled to the experimental temperature. When the temperature had stabilized at 350 °C, 2000 ppm NO and 5% O_2 in He were introduced at a rate of 200 ml/min for 20 min for NO adsorption. The NO concentration was monitored by a Vario Plus gas analyzer (MRU company, Germany).

H_2-TPR measurements were performed in a conventional flow apparatus. 200 mg sample was pretreated at an oxygen atmosphere by calcination at 600 °C for 1 h and subsequently cooled to 100 °C with helium flowing. Afterwards, 10% H_2/He flow (40 cm^3/min) was passed over the catalyst bed while the temperature was ramped from 100 °C to 900 °C at a heating rate of 10 °C/min. The hydrogen consumption signal was monitored by a thermal conductivity detector (TCD). Before the outlet gases entering the TCD, a cooling trap and a filter packed with molecular sieve 5A (60–80 meshes) were used to remove H_2O and CO_2.

3. Results

3.1. The catalytic activity measurement results

The TPO results of soot combustion over the Co_3O_4, $nmCeO_2$, and $Co_m/nmCeO_2$ catalysts are listed in Table 1. For comparison, the oxidation of bare soot was also included. The main product of soot combustion over these samples was CO_2, whereas both CO and CO_2 were the main products for soot uncatalytic combustion. The activity of Co_3O_4 for soot oxidation is low. It is possibly attributed to its large particle size and very low surface area. The nanoparticle $Co_m/nmCeO_2$ catalysts exhibited good catalytic activity for soot oxidation under the loose contact between soot and catalysts. As shown in Table 1, T_{50} decreased by more than 120 °C for soot combustion over nanometric CeO_2, and it was further lowered after Co supported on nanometric CeO_2. It indicated that supported cobalt oxide could further enhance the activity of catalysts. Among these catalysts, $Co_{20}/nmCeO_2$ gave the highest catalytic activity, i.e., the lowest T_{50} (368 °C). This temperature of soot combustion can ensure immediate activation of the catalyst on the filter under the condition of diesel engine emissions, whereas the same reaction under identical conditions required a temperature as high as 585 °C for the soot uncatalytic combustion. Therefore, these results indicated that nanometric CeO_2-supported cobalt oxide catalysts exhibited good catalytic performances for soot combustion. The BET surface areas of catalysts are also listed in Table 1. The surface area of Co_3O_4 (about 2 m^2/g) is very low. However, the high surface area of nanometric CeO_2 (about 50 m^2/g) is reasonable, considering that the prepared sample was of nanometer size. The cobalt oxides supported on nanometric CeO_2 decreases its surface area. However, it is noted that the catalytic activities follow a trend that is the inverse of that observed for the BET surface area of the catalyst. It indicated that there is no proportional correlation between the catalytic activities of catalysts and their surface areas. In other words, besides the surface area the other factors should play important roles in controlling the catalytic activity.

3.2. The results of XRD characterization

Fig. 1 shows the XRD patterns of Co_3O_4, $nmCeO_2$, and the various $Co_m/nmCeO_2$ samples. The XRD pattern of the pure $nmCeO_2$ exhibits a very strong peak at 2θ = 28.5° and other weak

Table 1
The BET surface areas of Co_3O_4, $nmCeO_2$, and $Co_m/nmCeO_2$ catalysts and their catalytic performances for the catalytic combustion of soot under loose contact conditions between the catalysts and soot (m = 0.1, 1, 4, 10, 20, 50, 100)

Catalysts	BET surface area/m^2/g	T_{10}/°C	T_{50}/°C	T_{90}/°C	$S^m_{CO_2}$/%
$Co_{0.1}/nmCeO_2$	43.5	377	456	498	92.8
$Co_1/nmCeO_2$	41.9	369	438	481	94.9
$Co_4/nmCeO_2$	40.5	347	412	468	96.6
$Co_{10}/nmCeO_2$	37.3	329	392	446	97.6
$Co_{20}/nmCeO_2$	34.2	286	368	418	98.8
$Co_{50}/nmCeO_2$	29.1	304	376	425	98.2
$Co_{100}/nmCeO_2$	24.7	315	384	437	98.1
$nmCeO_2$	48.8	379	465	516	90.4
Co_3O_4	1.9	340	495	546	91.5
Soot (without catalyst)	100.0	482	585	646	55.0

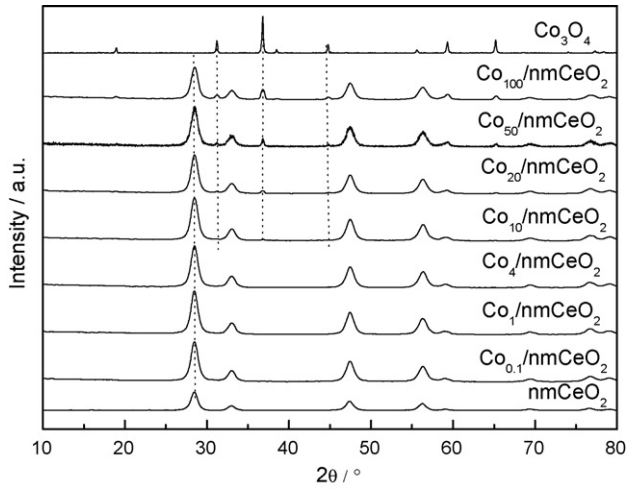

Fig. 1. The X-ray diffraction patterns of Co_3O_4, $nmCeO_2$, and $Co_m/nmCeO_2$ catalysts (m = 0.1, 1, 4, 10, 20, 50, 100).

peaks indicating the characteristics of fluorite structure, which is corresponding to a face-centered cubic (fcc) fluorite structure of CeO_2 (JCPDS Card No. 34–0394). For the $Co_m/nmCeO_2$ samples with low cobalt loading ($m < 10$), several obvious peaks, which reflect the characteristic of CeO_2, have been detected and no diffraction peaks due to crystalline CoO or Co_3O_4 are observed in the XRD patterns. It may be ascribed to the formation of Co–Ce–O solid solution or highly dispersed cobalt oxides on the surface of $nmCeO_2$ support [18]. When $m > 10$, several diffraction peaks at ~36.8° and 65.2° appeared in the XRD patterns due to the production of crystal phase of Co_3O_4 (JCPDS Card No. 78–1970). Compared to the $Co_m/nmCeO_2$ catalysts with different Co loadings, the characteristic fluorite CeO_2 peaks became wider with the increasing of Co loading, indicating that the crystallite sizes of catalysts become smaller. As shown in Table 2, the average crystallite sizes (D) of $Co_m/nmCeO_2$ catalysts determined with the Scherrer equation were in the range of 6–9 nm. However, the average crystallite size of pure Co_3O_4 is 39.7 nm. It indicates that nanometric cerium oxide support greatly enhanced the dispersion of cobalt oxide and decreased the crystalline size of Co_3O_4. Therefore, $Co_m/nmCeO_2$ catalysts should be able to exhibit better catalytic activity than Co_3O_4.

Fig. 2 shows SEM photographs of Co_3O_4, $Co_{20}/nmCeO_2$ and nanometric CeO_2 samples. It can be seen that the average particle size of Co_3O_4 is about 200 nm, thus nanometric particle Co_3O_4 sample cannot be produced by the auto-combustion method in this work. However CeO_2 and $Co_{20}/nmCeO_2$ nanopowders could be formed using the above preparation method at the caclined temperature of 600 °C for 6 h. The nanometric CeO_2 sample had an average particle size centered at around 20 nm with a spherical shape, and that of $Co_{20}/nmCeO_2$ sample is about 100 nm. The larger particle sizes observed from the SEM images than the crystallite sizes measured by XRD illustrates that powder particles were agglomerated to some extent.

Table 2
The average crystal parameters and crystal sizes of Co_3O_4, $nmCeO_2$, and $Co_m/nmCeO_2$ catalysts

Catalysts	Crystal face	I/I1	2θ/°	β/rad	D/nm	$(\varepsilon^2)^{1/2} \times 10^{-3}$
$Co_{0.1}/nmCeO_2$	111	100	28.504	0.0175	8.09	13.74
$Co_1/nmCeO_2$	111	100	28.4981	0.0169	8.40	13.24
$Co_4/nmCeO_2$	111	100	28.497	0.0169	8.36	13.30
$Co_{10}/nmCeO_2$	111	100	28.5038	0.0168	8.42	13.20
$Co_{20}/nmCeO_2$	111	100	28.5075	0.0175	8.08	13.76
$Co_{50}/nmCeO_2$	111	100	28.3747	0.0170	8.33	13.40
$Co_{100}/nmCeO_2$	111	100	28.5169	0.0170	8.31	13.38
Co_3O_4	311	100	36.8309	0.0036	39.72	2.18
$nmCeO_2$	111	100	28.449	0.0167	8.47	13.16

(m = 0.1, 1, 4, 10, 20, 50, 100).

3.3. The results of XPS characterization

Several typical catalyst samples were investigated by XPS with various levels of Co loading: 4, 20, and 100, and two sample oxides (Co_3O_4 and $nmCeO_2$) were also investigated for comparative purposes. The Co 2p, Ce 3d, and O 1s XPS spectra of the samples are shown in Fig. 3. In Fig. 3a, the Ce 3d peak positions agree with the data obtained for $nmCeO_2$. The Ce $3d_{5/2}$ lines, characteristic of the Ce(IV) oxidation state, are located at 882.3 eV, 889.0 eV, and 898.3 eV. The Ce $3d_{3/2}$ lines appear at 900.8 eV, 907.2 eV, and 916.6 eV. This complicated structure of the Ce 3d spectrum is determined by the electronic structure of cerium ions in the initial and final states [22]. Compared with the Ce 3d peak observed for the $nmCeO_2$ oxide support, the two weak XPS peaks located at 885.6 eV, and 904.0 eV were detected on the $nmCeO_2$-supported Co oxide samples suggesting the presence of Ce(III). It can be due to the deposition of cobalt oxide [18,22].

The Co 2p XPS spectra of $Co_m/nmCeO_2$ samples are compared with the one obtained for Co_3O_4 in Fig. 3b. The strongest photoelectron signals for cobalt arise from the $2p_{3/2}$ and $2p_{1/2}$ levels. The two XPS peaks of $Co_m/nmCeO_2$ ($2p_{2/3}$ = 779.9 eV and $2p_{1/2}$ = 795.2 eV) are due to the formation of bulk Co_3O_4. The higher energy positions of Co 2p peaks compared with Co_3O_4 are ascribed to the existence of more Co^{2+} in the catalysts than in the bulk Co_3O_4 [23]. This behavior is particularly evident in the samples with a lower cobalt-loading amount ($Co_4/nmCeO_2$). As the preparation procedure is the same for all the impregnated samples, the effect of CeO_2 in the stabilization of Co–O must be considered. Significantly, both CoO and CeO_2 are characterized by a cubic structure. Thus, at low cobalt loading, cobalt oxide may exist as CoO or cobalt–cerium solid solution. Compared with the low cobalt loading samples, the decrease of binding energy suggests the increase of Co_3O_4 content in the catalysts with higher Co/Ce nominal atomic ratio [18,24]. The literature reported that the sharp and more intense component at lower binding energy is ascribed to Co^{3+}, whereas the shoulder at higher binding energy represents the Co^{2+} component. This is not surprising. It is well known that for oxidic compounds containing both Co(II) and Co(III) ions there is an inverse shift in the main peak position of the Co^{2+} and Co^{3+}. This anomaly may be regarded as effect of a large decrease in ionicity (or, reversely, of a large increase in covalency) of the Co^{3+}–O bonding with respect to the Co^{2+}–O bonding in the crystal lattice [23].

As shown in Fig. 3c, the position of the O 1s XPS peaks in the $Co_m/nmCeO_2$ samples (~529.4 eV) agree with the expected value for oxygen in ceria. A shoulder peak shows a higher BE (~531.6 eV) attributing to oxygen in the form of –OH or as O^- [18,25]. The lower hydroxylation of the nanocomposites with respect to CeO_2, evidenced by the comparison of the corresponding O 1s XPS spectra, could indicate the grafting of cobalt oxide to CeO_2 by condensation of OH groups [25].

3.4. The results of Raman characterization

The Raman spectroscopic technique has been used for the investigation of the structures of the fresh catalysts, and the spectra obtained are compiled in Fig. 4. For comparison, the Raman spectrum of Co_3O_4 is also included in this figure. The absorption peak at around 462 cm^{-1} is attributed to the F_{2g} Raman active

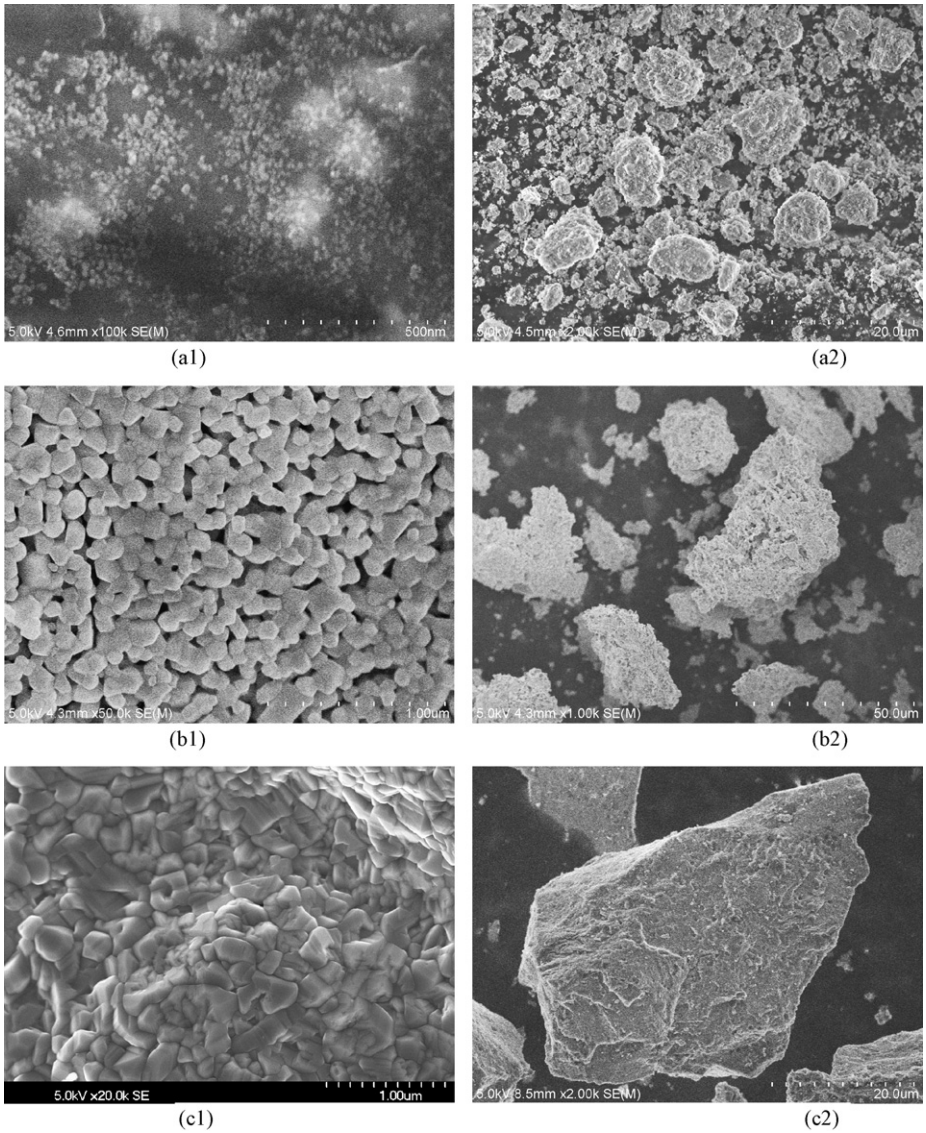

Fig. 2. The SEM photographs of three catalysts. (a1) and (a2): $nmCeO_2$, (b1) and (b2): $Co_{20}/nmCeO_2$, (c1) and (c2): Co_3O_4.

mode of fluorite structure in CeO_2 [26,27]. Fluorite-structure is a cubic structure (fcc) in which the cations are placed in the corners and in the centres of faces and oxygen atoms are located at the tetrahedral sites. The Raman spectra for these fluorite-type oxide structures are dominated by oxygen lattice vibrations and are sensitive to crystalline symmetry [27]. The presence of low valence cobalt ions in the CeO_2 lattice deforms the structure, and the fluorite-characteristic peak intensity decreases significantly with Co loading. It has been reported that this deformation favors oxygen mobility, affecting the redox behavior of the material [27,28]. As shown in Fig. 4, at low Co content, no Co_3O_4 crystal phase was present on the catalyst surface, and the medium or high Co content results in the appearance of the absorption peak at 692 cm^{-1} which can be assigned to the stretching vibration of Co–O in the spinel Co_3O_4 [29].

3.5. The results of UV–vis DRS characterization

The UV–vis DRS spectroscopy can be applied to investigate the structures of supported oxide catalysts due to the ligand-to-metal charge transfer (LMCT) transitions of transitional metal ions in the 200–500 nm region and d–d transition bands in the 600–800 nm region due to d–d electron transferring. The DRS spectral features are sensitive to nano-sized oxide particle. The existence of Co_3O_4 is further confirmed by the DRS spectroscopy. The DRS spectra of nanometric CeO_2-supported CoO_x catalysts using nanometric CeO_2 support as reference sample are shown in Fig. 5. Both maximal characteristic bands at 720 nm and 470 nm are due to the formation of Co_3O_4 where a charge transfer via octahedral sites occurs [30]. Herein it is worth noting that these bands become more intense as the cobalt loading of catalyst increases. For low cobalt loading sample especially $Co_{0.1}/nmCeO_2$, no d–d transition bands originating from surface Co^{2+}/Co^{3+} species in the UV–vis region (600–800 nm) were observed. For high cobalt-loading sample, an intense absorption band centered at about 720 nm, indicating some surface Co^{2+}/Co^{3+} species existing in the Co_3O_4.

3.6. The results of IR characterization

In consistence with the Raman results described above, FT-IR spectroscopy gave some information about the surface compositions and structures of the catalysts. Fig. 6 shows the FT-IR spectra

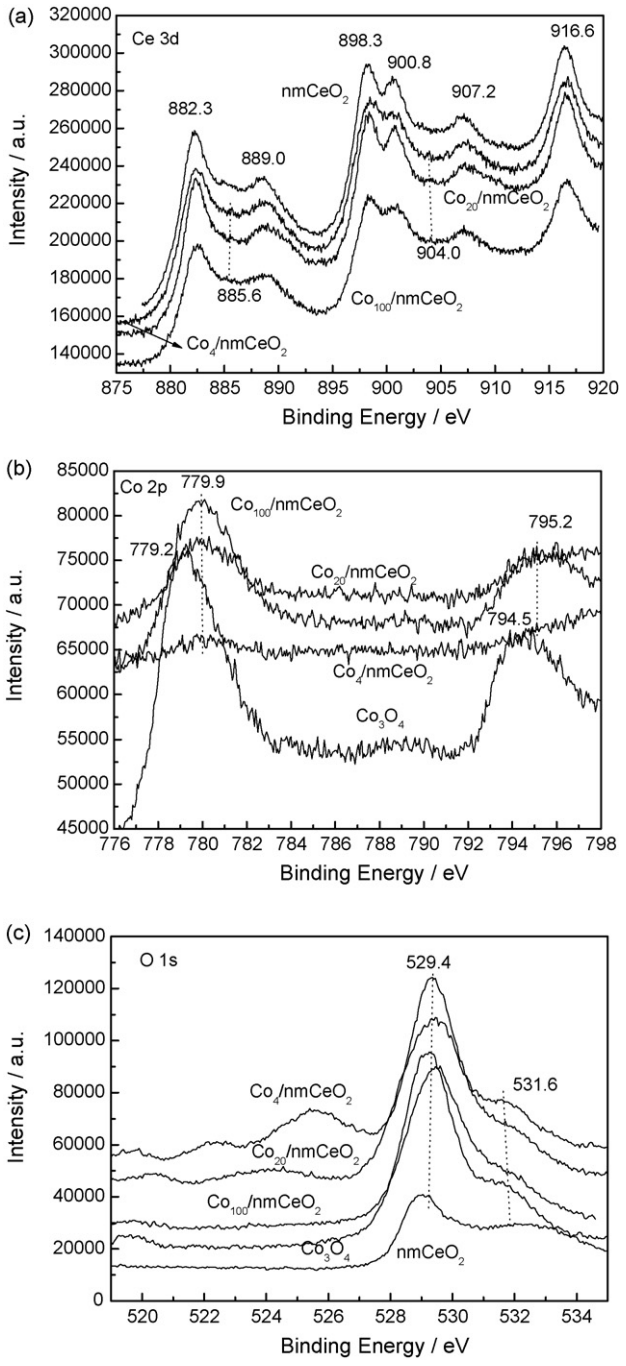

Fig. 3. Ce 3d, Co 2p, and O 1s XPS spectra of the $Co_m/nmCeO_2$, $nmCeO_2$, and Co_3O_4 catalysts (m = 4, 20, 100): (a) Ce 3d XPS spectra, (b) Co 2p XPS spectra, (a) O 1s XPS spectra.

of the $Co_m/nmCeO_2$ oxides, and the spectra of Co_3O_4 and $nmCeO_2$ are also shown in Fig. 6 for comparison. The spectra of the $Co_m/nmCeO_2$ oxides with low cobalt loading show strong absorption bands below 600 cm^{-1} and it can be assigned to the Ce–O lattice vibration of cubic fluorite structure in CeO_2 [31]. All samples except nanometric CeO_2 show two distinct bands at ca. 570 cm^{-1} (ν_1) and 663 cm^{-1} (ν_2) that are due to the stretching vibrations of the Co–O bond of cobaltic oxide. The ν_1 band is the characteristic vibration of Co^{3+} in octahedral holes and the ν_2 band is attributed to the vibration of Co^{2+} in tetrahedral holes [32]. The presence of these bands is in accordance with the structure of CoO_x (spinel for Co_3O_4 and face-centered cubic for CoO).

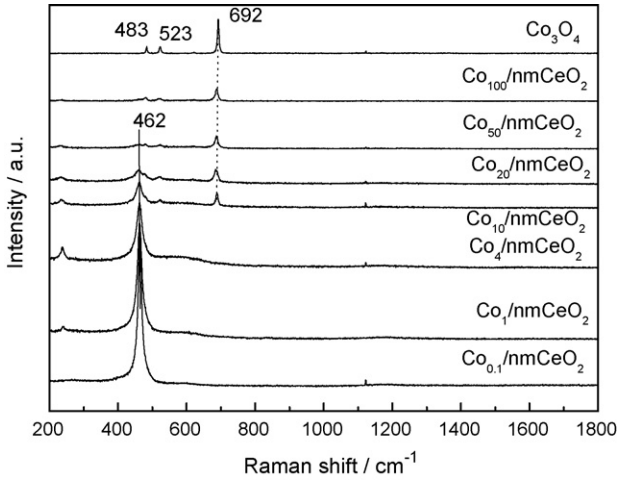

Fig. 4. The Raman spectra of Co_3O_4, $nmCeO_2$, and $Co_m/nmCeO_2$ catalysts (m = 0.1, 1, 4, 10, 20, 50, 100).

The in situ DRIFT spectra during exposure of $Co_m/nmCeO_2$ catalysts to 2000 ppm NO and 5% O_2 at 350 °C are shown in Fig. 7a. The adsorbed species are attributed predominantly to various nitrites and nitrates, as well as other nitrogen-containing species. A strong absorption band at ~1236 cm^{-1} is assigned to the bridging bidentate nitrite, and two shoulder peaks at 1540 cm^{-1} and 1558 cm^{-1} are due to $\nu_{N=O}$ stretching vibration of chelating bidentate nitrates. The peak located at ~1004 cm^{-1} is attributed to the symmetric stretching vibration of bidentate nitrates, and a weak peak located at about 1352 cm^{-1} is ascribed to the symmetric stretching vibration of monodentate nitrates (ν_{symNO_2}) [33–37]. For the catalysts with different Co-loading amounts, their absorption peak positions are basically same. However, their relative adsorption amounts, i.e., the IR peak intensities, are different and dependent on the catalyst composition. As shown in Fig. 7a, there are very small peaks of NO_x adsorbed for nanometric CeO_2 sample, and the introduction of Co into catalysts enhances the NO_x adsorption on these catalysts. The intensities of the several strong peaks at 1004 cm^{-1}, 1236 cm^{-1}, 1540 cm^{-1} and 1558 cm^{-1} are enhanced with the increasing of Co-loading amount until m is equal to 20.

Fig. 7b shows the in situ DRIFT spectra of $Co_{20}/nmCeO_2$ catalyst for NO_x adsorption in (2000 ppm NO + 5% O_2)/He atmosphere as a

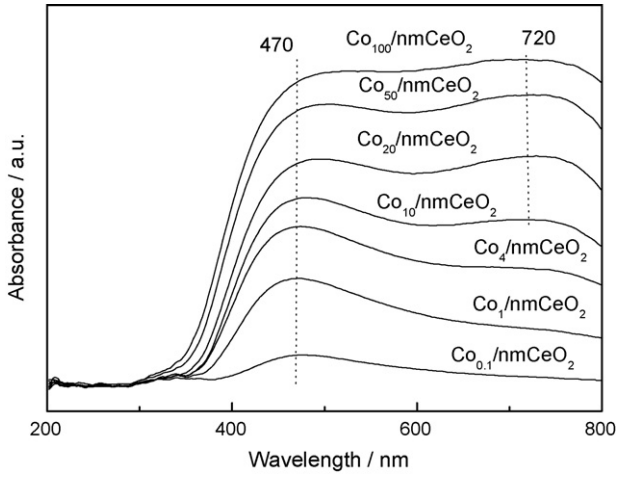

Fig. 5. The UV–vis spectra of $Co_m/nmCeO_2$ catalysts (nanometer CeO_2 support was used as reference baseline; m = 0.1, 1, 4, 10, 20, 50, 100).

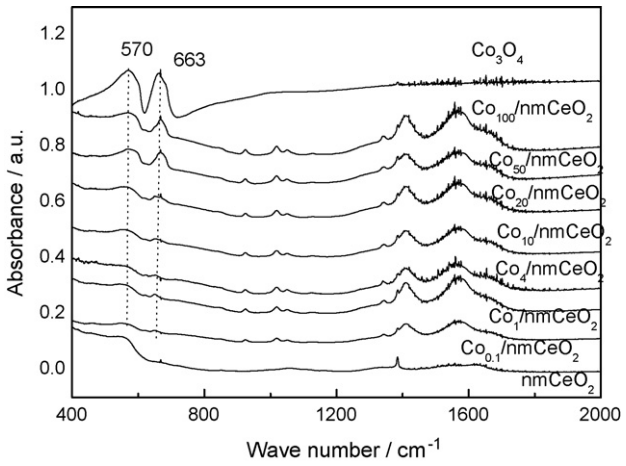

Fig. 6. The FT-IR spectra of Co_3O_4, $nmCeO_2$, and $Co_m/nmCeO_2$ catalysts (m = 0.1, 1, 4, 10, 20, 50, 100).

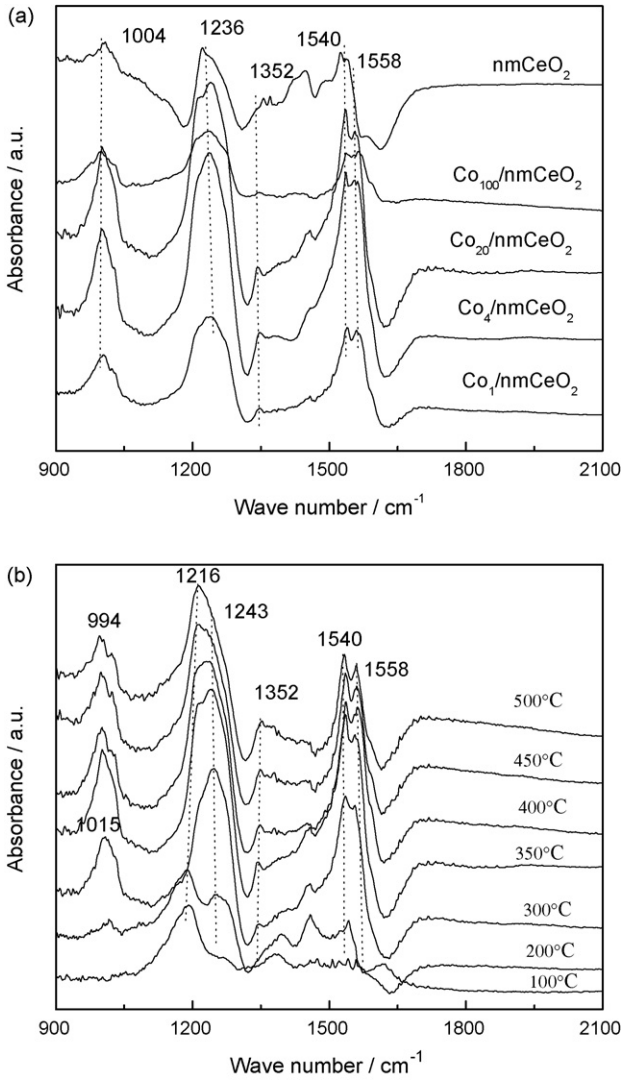

Fig. 7. The in situ DRIFT spectra of NO_x adsorption over $nmCeO_2$ and $Co_m/nmCeO_2$ catalysts (m = 1, 4, 20, 100) (a) $nmCeO_2$ and $Co_m/nmCeO_2$ at 350 °C and (b) $Co_{20}/nmCeO_2$ at different temperatures.

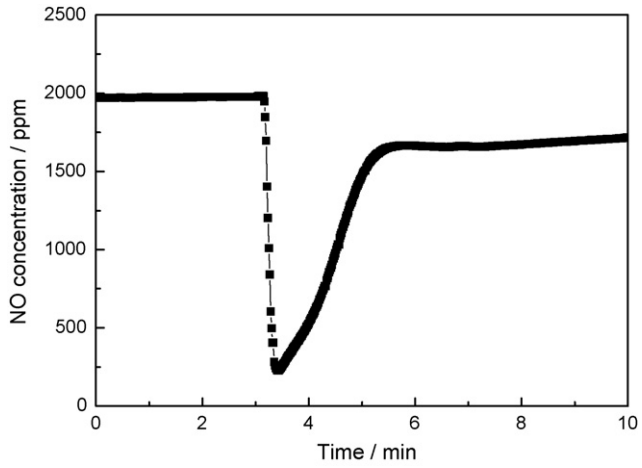

Fig. 8. NO adsorption on $Co_{20}/nmCeO_2$ at 350 °C.

function of temperature. The main absorption bands locate at 994 cm^{-1}, 1216–1243 cm^{-1}, 1352 cm^{-1}, 1540 cm^{-1}, and 1558 cm^{-1} indicating the presence of the adsorbed species which can be assigned to various kinds of nitrites and nitrates. At 100 °C the peak intensities of NO_x adsorption are very low in the IR spectrum, and with the increasing of adsorption temperature, the intensities of IR adsorption peaks are gradually enhanced. However, they almost keep constant after adsorption temperature reached 350 °C. It indicates that the optimal temperature range is 300–400 °C for NO_x adsorption on $Co_{20}/nmCeO_2$ sample.

3.7. The results of NO adsorption and oxidation on $Co_{20}/nmCeO_2$ catalyst

The adsorption profile of NO on $Co_{20}/nmCeO_2$ catalyst is presented in Fig. 8. The NO concentration rapidly decreases at the beginning due to the NO adsorption on the sample and gains the equilibrium only after 3 min attributing to the NO adsorption saturation. However, the equilibrium concentration of NO adsorption does not obtain the initial concentration. It may be ascribed to part NO transferring to NO_2. It would be clearly confirmed by the following NO oxidation experiments.

Fig. 9 exhibits the NO oxidation profile on $Co_{20}/nmCeO_2$ catalyst. For comparison, the NO_2 concentration profiles of NO oxidation on nanometric CeO_2 and without catalyst are also displayed on the figure. As shown in Fig. 9, the direct evidence of

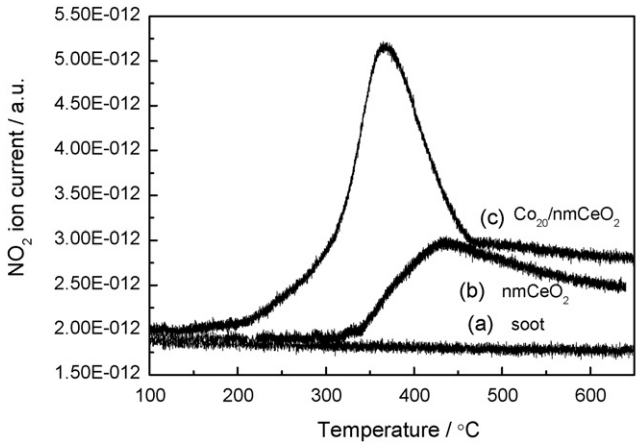

Fig. 9. The outlet NO_2 concentration plots over soot, $nmCeO_2$, and $Co_{20}/nmCeO_2$.

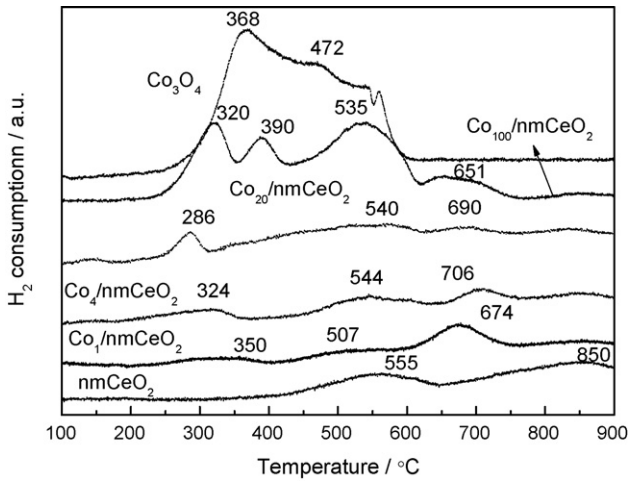

Fig. 10. The H_2-TPR curves of Co_3O_4, $nmCeO_2$, and $Co_m/nmCeO_2$ catalysts (m = 1, 4, 20, 100).

NO_2 produced on $Co_{20}/nmCeO_2$ catalyst is detected by the means of mass spectroscopic measurement. Almost no NO_2 was detected in the case of no catalyst when combustion temperature was less than 600 °C, as shown in plot (a). However, when nanometric CeO_2 was present, the NO_2 concentration remarkably increased, as shown in plot (b). The NO_2 concentration was largest on a typical catalyst ($Co_{20}/nmCeO_2$), as shown in plot (c).

3.8. The results of H_2-TPR

The reducibility of metallic ion can be reflected by H_2-TPR measurement. Thus, H_2-TPR results can also reflect the redox ability of metal oxide catalysts. In this work, the reduction peak temperature (T_{red}) was taken as a measure of the reducibility of the catalyst system. The lower T_{red} is, the stronger is the redox ability of catalysts. Since in practical applications the rate of soot oxidation at lower temperatures is more important than that at higher temperatures, we especially focus on the lowest T_{red} of H_2-TPR. Fig. 10 exhibits the H_2-TPR results of Co_3O_4, nanometric CeO_2, and various nanometric CeO_2-supported cobalt oxides. The profile of pure nanometric CeO_2 shows two weak peaks centered at 555 °C and 860 °C, respectively. They are attributed to the reduction of the surface oxygen and lattice oxygen of nanometric CeO_2 [38]. In contrast to a pure Co_3O_4 crystalline undergoes the reduction at about 368 °C (and a shoulder peak at about 472 °C). Thus, the redox ability of Co_3O_4 is better than that of nanometric CeO_2. However, compared with that of pure Co_3O_4 in the case of $Co_m/nmCeO_2$ supported oxides with different Co/Ce atomic ratios, the reduction peaks are all shifted to lower temperature in the H_2-TPR profiles. The presence of Co decreases the lowest T_{red} from 555 °C (nanometric CeO_2) to 286 °C ($Co_{20}/nmCeO_2$). Among these catalysts, $Co_{20}/nmCeO_2$ displays the lowest reduction temperature in the H_2-TPR profiles, which is in good agreement with its best catalytic activity. It is noticed that the total amounts of H_2 consumed during TPR increased with the increasing of Co/Ce atomic ratio. This phenomenon is due to the content of cobalt increasing in the catalyst mass per unit, and the reduction of cobalt oxides would consume more hydrogen than that of CeO_2.

4. Discussion

4.1. The influence of the redox property of catalysts

The reaction of soot combustion is a kind of deep oxidation reaction. The catalysis nature of the reaction is redox process. Therefore, the redox property of the catalyst determines its intrinsic activity. The redox ability of CeO_2 is the strongest among various ordinary metal oxide supports such as Al_2O_3, SiO_2, CeO_2, and TiO_2, etc. Thus, CeO_2 is an appropriate support for soot combustion over supported oxide catalysts. As far as the active component of catalyst is concerned, Co_3O_4 shows very high oxidation activity. Thus, nanometric CeO_2-supported cobalt oxide catalysts have very excellent intrinsic activities for soot combustion. As shown in H_2-TPR and the catalytic activity measurement results, the change of the reduction peak temperatures in the H_2-TPR profiles of $Co_m/nmCeO_2$ supported oxides with different Co/Ce atomic ratios are consistent with their catalytic activity measurement results. Among these catalysts, $Co_{20}/nmCeO_2$ displayed the lowest reduction temperature in the H_2-TPR profiles, and thus it also exhibited the best catalytic activity.

It is well known that the redox pair of Ce^{4+}/Ce^{3+} is the basis of the catalytic activity for CO and HC oxidation by NO_x and O_2 in the CeO_2-containing catalyst designed for TWC. Imanaka et al. [39] reported the important role of doping Bi and/or loading Ag in improving this redox process. The redox behavior studied by H_2-TPR in this work demonstrates that the loading of Co cations can remarkably enhance the redox ability of catalysts. It can be expected that the rate of active oxygen generated by the catalyst reaction with soot is much faster than the rate of its combination giving gas-phase O_2. The creation of such active oxygen species will decrease the soot oxidation temperature. For example, $Co_{20}/nmCeO_2$ produces more such active species, leading to 98.8% selectivity of CO_2 production at T_m compared with 90.4% over nanometer CeO_2 alone. Raman spectra indicate that this improvement is related to the deformation of the CeO_2 structure, which increases the oxygen mobility on the lattice and favors the Ce^{4+}/Ce^{3+} cycle. XPS results indicate that the loading of cobalt promotes the production of Ce^{3+} and thus enhances $Ce^{4+} \leftrightarrow Ce^{3+}$ redox process. And the oxygen mobility is also changed by the form of –OH or as O^-. On the other hand, Uner et al. [12] reported that the pronounced activity of cobalt oxide catalysts seems to stem form the reducibility of the oxide itself. In the presence of another reducible oxide such as CeO_2, the oxygen needed for the oxidation reaction would be provided by the second oxide. It would result in the very low peak combustion temperatures for soot, when compared with similar catalysts supported over other oxide supports. A spillover mechanism at the cobalt oxide–ceria interface is postulated to be the main mechanism for soot oxidation. The bulk oxide properties may be altered when solid solutions are formed during the catalyst preparation. The generation of "active oxygen" induced by Co cations, explains the high activity of the $Co_m/nmCeO_2$ catalysts in relation to CeO_2. This improvement in soot conversion over $Co_m/nmCeO_2$ catalysts can be attributed to the loading of cobalt oxides. Moreover, the high oxygen mobility offered the other advantage. It is possible to produce relatively high amounts of CO during soot combustion because the oxygen amounts in air can be quickly depleted. The CO formation would cause an additional environmental problem. However, the highly mobile oxygen existed in the catalysts may offer the part oxygen for soot oxidation thus decrease the CO amount. Therefore, this kind of mixed oxides with high oxygen mobility may be very important in oxidation reaction and catalysis application.

It is noted that a linear relationship is not observed between the BET surface areas of the catalysts and their catalytic activities under loose contact conditions. This suggests that the BET surface area is not the main determining factor affecting the activity of the catalysts, and some other factors such as active oxygen and the contact between soot and catalysts might play an important role. Under loose contact conditions, it seems appropriate to assume that most of the active oxygen generated by the catalyst is not

useful for soot oxidation. The transport of active oxygen from catalysts to soot particles seems not to be a problem under tight contact conditions, but loose contact between catalyst and soot particles makes it difficult for the "active oxygen" transfer to soot. However, it is loose contact between the catalysts on the surface of filter and soot particles under practical conditions. Therefore, searching new catalytic materials to improve the contact between soot and catalyst is an important work. Nanometric catalysts prepared in this study will provide an option to enhance the loose contact activity for soot combustion.

4.2. The influence of the nanometer size

As we consider the results of this study, two challenges remain for future research: to design appropriate catalytic materials that possess strong redox ability, and to design new systems that improve the contact between soot and catalyst. The efficiency of a catalyst is strongly influenced by the contact between soot and catalyst. Though by using many other mechanical methods, such as ball milling, mechanic mixing, part of the catalyst particles may be contacted with soot materials, this method gave only tight contact condition between soot and catalyst. The condition cannot be easily obtained under the real exhaust gases emitted from diesel engine. Therefore, the catalytic effect is weakened in the real application. In order to intensify the catalytic effect, nano-particle catalysts may be used. Since the nano-particle catalysts have higher fraction of surface atoms than the conventional catalysts with large particle size, the catalyst is in close proximity with soot particle and more catalyst surface is exposed to reaction atmosphere. A decrease in particle size from 1 μm to 10 nm will increase the probability of contact each other by 100 times. For a given catalyst, the more the surface of catalyst is exposed to soot, the stronger the catalytic effect. Therefore, the catalytic effect of nano-particle catalyst will be stronger than that of the big particles when the same amount of catalysts is used. And lower amounts of catalysts are needed when the catalyst is in nano-particles compared to the big catalyst particles for the same level of catalytic effect [40]. Using smaller amounts of catalysts can effectively combust soot particle (that can be reached in relatively short time) and decrease the total cost of the materials. By using the method developed in this work, all the catalysts particles are deposited on the surface of nanometric CeO_2 support. The particle size of the catalysts in this work is about tens of nanometer, which is much smaller than that of the supported-oxide catalysts prepared by conventional methods. Therefore, the catalysts of cobalt oxides dispersed on the surface of naometric CeO_2 support should have highly catalytic activity.

The nanometric CeO_2 support was prepared by the auto-combustion method assisted by rotating evaporation. After the formation of the precursor solution, most of water in the solution was quickly evaporated by rotating evaporation at $P = 0.02$ MPa vacuum. Not only could it prevent from the further agglomeration of solute ions, but also avoided the sudden boiling of the solution. On the other hand, most of water was evaporated at low temperature and in short time, thus nitrate ions were kept in the solution. There are two functions of citric acid during the synthesis. Firstly, it acted as a complex agent for the cations in the nitrate solution. Secondly, it was the fuel during the following combustion. To control the combustion reaction, the ratio of fuel (citric acid) to oxidizer (nitrate) can be varied. During the combustion synthesis process a red brownish-colored gas was observed indicating the formation of NO_x besides the gaseous species of H_2O, CO_2 and N_2. It was beneficial to producing a great amount of gases during combustion synthesis. They limit the contact of particles, and hence prevent from agglomeration of the powder particles. Therefore, it would be favorable for the formation of nanopartilce CeO_2 catalyst. A desired homogenous powder can be produced in a short time at low cost and with simple equipment. However, nanoparticle Co_3O_4 sample cannot be obtained by the same preparation method. It may be due to cobalt oxide more easily produced spinel complex oxides and the combination is tighter between their atoms or molecules. Thus, Co_3O_4 easily formed the particles with larger size during auto-combustion. After nanometric CeO_2 support was prepared, the cobalt oxides were supported over the nanometric support by the method of ultrasonic-assisted incipient-wetness impregnation. It would be beneficial to enhancing the dispersion of cobalt oxides over the support. Therefore, the nanometric particle Co_m/nmCeO_2 catalysts can be obtained.

4.3. The influence of NO_2

It is necessary to remove the soot PM from the filter otherwise it would simply become blocked and useless. A strategy developed by Johnson Matthey for their DPF is to use the oxidizing properties of NO_2 to combust the PM. NO_2 is a much more effective oxidant than O_2 so that, providing a sufficient concentration of NO_2 in the exhaust, the removal of PM can be performed at lower temperatures [41]. In the continuously regenerating trap system the removal of PM by oxidation with NO_2 is achieved by placing an oxidation catalyst upstream of the trap in order to convert NO in the exhaust into NO_2. Oi-Uchisawa et al. [9,10] reported that a platinum catalyst could oxidize NO to NO_2, which subsequently oxidize soot to CO and CO_2. So, NO_2 is used as intermediate to facilitate an indirect contact between the platinum catalyst and soot. This mechanism subtly changed solid(soot)–solid(catalyst) contact into solid(soot)–gas(NO_2)–solid(catalyst) contact. Thus, the platinum catalyst system obtained the best results so far reported for soot combustion under loose contact conditions. The high oxidation rate of soot is due to the strong oxidizing ability of NO_2. A similar mechanism is found for soot combustion over nanometric CeO_2-supported cobalt oxide catalysts in this study. As shown in Fig. 9, the direct evidence of NO_2 produced is detected by the means of in situ mass spectroscopic measurement. According to the results of in situ DRIFT, NO adsorption experiment and in situ mass spectroscopy detection, it was found that NO is oxidized to NO_2 over the catalyst, which is stored on the catalyst as nitrite/nitrate. The nitrates can decompose and release NO_2 to the gas phase or the NO is directly oxidized to NO_2 in the gas phase. Then, NO_2 acts as the oxidizing agent for soot combustion. The nitrate storage capacity of Co_{20}/nmCeO_2 is three to five times higher than that of the bare nmCeO_2 oxide resulting in a major contribution of the produced NO_2 to the soot oxidation process. This explains the strong synergistic effect of cobalt and cerium in the mixed oxide on the soot oxidation.

The obtained DRIFT spectra (Fig. 7) of adsorbed species are in a good agreement with the results described in the literature [33–37]. The strong adsorption peaks only observed for the mixed oxides correlate well with high NO_x storage capacity of the mixed oxides compared with that of the individual oxides. The identification of the adsorbed species proves that NO_x is stored in form of nitrite/nitrates on the catalyst surface, for which NO must be partially oxidized to NO_2 in a preceding step. This also explains why NO_2 can be released from the catalyst at higher temperatures. The NO adsorption experiment on Co_{20}/nmCeO_2 catalyst (Fig. 8) shows that the NO uptake drops rapidly and almost full saturation is achieved within less than 3 min. It is suggestive of NO being stored only on the surface and not transferred to the bulk in a slow diffusion process. The storage of NO_x on the surface and not in the bulk of the catalyst would be further beneficial to the production of NO_2 [42].

In order to provide some insights into the NO_x promotion function for the soot combustion NO oxidation experiments were carried out. The NO_2 concentration in the outlet gas mixture is plotted as a function of temperature in Fig. 9. It is important to note that the NO_2 level in the gas stream is very little at the entrance of the reactor, with NO being the main component of the NO_x binary. NO can be oxidized to NO_2 by O_2 according to the reaction NO + 1/2 $O_2 \rightarrow NO_2$. The predicted NO_2 level considering the thermodynamic equilibrium of this reaction was described in literature [43]. As shown in Fig. 9, soot exhibited no activity for NO_2 production, and the NO_2 level reached with soot is the same as that measured in the initial time of the reaction. In comparison, nanometric CeO_2 was quite effective for NO oxidation to NO_2 from 300 °C. The NO_2 profile obtained with this catalyst increased with temperature until the thermodynamic equilibrium of the above equation was fulfilled, and then decreased at higher temperatures following thermodynamics. The highest NO_2 concentration was reached at 450 °C. Fig. 9 further shows that the NO_2 concentration was much larger on $Co_{20}/nmCeO_2$ catalyst than that on nanometric CeO_2. At the same time, the peak temperature of the production of NO_2 on $Co_{20}/nmCeO_2$ catalyst is about 365 °C, which is much lower than that on nanometric CeO_2. In fact, the strong oxidation ability of $Co_{20}/nmCeO_2$ for NO oxidation is consistent with the results of H_2-TPR as shown in Fig. 10. Thus, $Co_{20}/nmCeO_2$ catalyst should have more excellently catalytic activity for soot combustion.

In summary, based on the above results and discussion, the following three reasons can lead to the highly catalytic activities of nanometric CeO_2-supported cobalt oxides for soot combustion. First of all, the catalysis nature of soot oxidation is redox process. The redox property of the catalyst determines its intrinsic activity. Both nanometric CeO_2 support and Co_3O_4 active component possess strong redox ability. Therefore, the intrinsic activities of nanometric CeO_2-supported cobalt oxide catalysts are very good. Secondly, the contact between catalyst and soot is a necessary external condition which is significantly important for the catalyst to play the role of catalysis. The good contact between the catalyst and soot can be obtained by synthesizing nanometric CeO_2-supported cobalt oxide catalysts. It is because that the surface particle sizes of nanoparticle catalyst are small. Surface atoms on surface of nanoparticle catalysts have extra and high surface energies and they are good at mobility. Thirdly, similarly to noble metal Pt catalysts, nanometric CeO_2-supported cobalt oxides can efficiently catalyze the NO to NO_2. And the oxidizing ability of NO_2 is much stronger than that of O_2 and it can directly oxidize the soot particle to CO_2 and ensure the good indirect contact performances between catalysts and soot particles. Thus, the oxidation temperature of soot becomes lower even under loose contact conditions. In general, the catalytic activities of nanometric CeO_2-supported cobalt oxide catalysts prepared in this study are very high for soot combustion under loose contact conditions between soot and the catalyst. The best catalytic activity was obtained over $Co_{20}/nmCeO_2$ catalyst, and its catalytic activity for the combustion of soot particle is as good as supported Pt catalysts, which is the best catalyst system so far reported for soot combustion under loose contact conditions.

5. Conclusions

1. The nanometric CeO_2 particles were obtained by the method of auto-combustion, and the nanometric CeO_2-supported cobalt oxide catalysts were prepared by the means of ultrasonic-assisted incipient-wetness impregnation. Their structures were altered with the loading amount of the Co. At low Co loading, cobalt oxide existed as CoO or cobalt–cerium oxide solid solution, and the medium or high Co loading resulted in the presence of spinel Co_3O_4. While higher Co loading amount caused the conglomeration of the Co_3O_4 crystalline, leading to the lower activity for soot catalytic combustion.
2. In the $Co_m/nmCeO_2$ catalysts, the introduction of Co remarkably enhanced the catalytic activity, which is due to the strong redox ability of cobalt oxide and the loading of cobalt enhances the redox process of $Ce^{4+} \leftrightarrow Ce^{3+}$. Among these catalysts, $Co_{20}/nmCeO_2$ displays the lowest reduction temperature in the H_2-TPR profiles, which is in good agreement with its best catalytic activity.
3. The results of NO adsorption, in situ DRIFT spectra, and in situ mass spectra indicate that NO can be adsorbed and oxidized on the $Co_m/nmCeO_2$ catalysts. The adsorbed species existed on the catalyst surface in the form of nitrite/nitrates, and it is important that the adsorption NO was stored only on the surface and not transferred to the bulk of catalysts. Thus, NO_2 can be generated from nitrates decomposition and releasing NO_2 or NO directly catalytic oxidation to NO_2 in the gas phase on $nmCeO_2$ and $Co_{20}/nmCeO_2$ catalysts, which was confirmed by mass spectroscopic measurement results. Due to the strong oxidizing ability of NO_2 and the good contact property of NO_2 molecule and soot particles, the soot combustion rate was accelerated. Moreover, the surface particle sizes of nanometric $Co_m/nmCeO_2$ catalysts are small and their surface atoms have extra and high surface energy. Thus, their surface atoms are good at mobility. In other words, the nanometric $Co_m/nmCeO_2$ catalysts can provide the good contact conditions between soot and catalysts. Therefore, the nanometric $Co_m/nmCeO_2$ oxides have good catalytic activities for soot combustion under loose contact conditions between soot and the catalyst. The best catalytic activity was obtained over $Co_{20}/nmCeO_2$ catalyst (T_{50} = 368 °C). This catalytic activity for the combustion of soot particle is as good as supported Pt catalysts, which is the best catalyst system so far reported for soot combustion under loose contact conditions.

Acknowledgements

This work was supported by the National Natural Science Foundation of China (No. 20773163, 20473053 and 20525621), the Beijing Natural Science Foundation in China (No. 2062020), the 863 program of China (No. 2006AA06Z346), and the Scientific Research Key Foundation for the Returned Overseas Chinese Scholars of State Education Ministry.

References

[1] Z.P. Liu, S.J. Jenkins, D.A. King, J. Am. Chem. Soc. 126 (2004) 10746.
[2] J. Liu, Z. Zhao, C. Xu, A. Duan, L. Zhu, X. Wang, Appl. Catal. B 61 (2005) 39.
[3] W.F. Shangguan, Y. Teraoka, S. Kagawa, Appl. Catal. B 8 (1996) 217.
[4] Y. Teraoka, K. Nakano, S. Kagawa, Appl. Catal. B 34 (2001) 73.
[5] S.S. Hong, G.D. Lee, Catal. Today 63 (2000) 397.
[6] K. Krishna, A. Bueno-López, M. Makkee, J.A. Moulijn, Appl. Catal. B 75 (2007) 210.
[7] J. Liu, Z. Zhao, C. Xu, A. Duan, T. Meng, X. Bao, Catal. Today 119 (2007) 267.
[8] J.P.A. Neeft, W. Schipper, G. Mul, M. Makkee, J.A. Moulijn, Appl. Catal. B 11 (1997) 365.
[9] J. Oi-Uchisawa, S. Wang, T. Nanba, A. Ohi, A. Obuchi, Appl. Catal. B 44 (2003) 207.
[10] J. Oi-Uchisawa, A. Obuchi, S. Wang, T. Nanba, A. Ohi, Appl. Catal. B 43 (2003) 117.
[11] K. Hinot, H. Burtscher, A.P. Weber, G. Kasper, Appl. Catal. B 71 (2007) 271.
[12] D. Uner, M.K. Demirkol, B. Dernaika, Appl. Catal. B 61 (2005) 334.
[13] J. Liu, Z. Zhao, P. Liang, C. Xu, A. Duan, G. Jiang, W. Lin, I.E. Wachs, Catal. Lett. 120 (2008) 148.
[14] V. Palma, P. Russo, G. Matarazzo, P. Ciambelli, Appl. Catal. B 70 (2007) 254.
[15] J. Liu, Z. Zhao, C. Xu, A. Duan, Appl. Catal. B 78 (2008) 61.
[16] H.J. Kwon, J.H. Baik, Y.T. Kwon, I.-S. Nam, S.H. Oh, Chem. Eng. Sci. 62 (2007) 5042.
[17] D.C. Sayle, S.A. Maicaneanu, G.W. Watson, J. Am. Chem. Soc. 124 (2002) 11429.
[18] M.M. Natile, A. Glisenti, Chem. Mater. 17 (2005) 3403.

[19] P.G. Harrison, I.K. Ball, W. Daniell, P. Lukinskas, M. Céspedes, E.E. Miró, M.A. Ulla, Chem. Eng. J. 95 (2003) 47.
[20] H. Wang, Z. Zhao, C. Xu, J. Liu, Catal. Lett. 102 (2005) 251.
[21] X. Chen, S.S. Mao, Chem. Rev. 107 (2007) 2891.
[22] M.Y. Smirnov, A.V. Kalinkin, A.V. Pashis, A.M. Sorokin, A.S. Noskov, K.C. Kharas, V.I. Bukhtiyarov, J. Phys. Chem. B 109 (2005) 11712.
[23] G. Fierro, M. Lo Jacono, M. Inversi, R. Dragone, P. Porta, Top. Catal. 10 (2000) 39.
[24] F. Morales, F.M.F. Groot, O.L.J. Gijzeman, A. Mens, O. Stephan, B.M. Weckhuysen, J. Catal. 230 (2005) 301.
[25] M. O'Connell, A.K. Norman, C.F. HuÈttermann1, M.A. Morris, Catal. Today 47 (1999) 123.
[26] B.M. Reddy, A. Khan, P. Lakshmanan, M. Aouine, S. Loridant, J.C. Volta, J. Phys. Chem. B 109 (2005) 3355.
[27] B.M. Reddy, A. Khan, Y. Yamada, T. Kobayashi, S. Loridant, J.C. Volta, J. Phys. Chem. B 107 (2005) 11475.
[28] L. Dong, Y. Hu, M. Shen, T. Jin, J. Wang, W. Ding, Y. Chen, Chem. Mater. 13 (2001) 4227.
[29] E. Widjaja, J.T. Sampanthar, X. Han, E. Goh, Catal. Today, in press.
[30] C. Tang, C. Kuo, M. Kuo, C. Wang, S. Chien, Appl. Catal. A 309 (2006) 37.
[31] A. Bumajdad, M.I. Zaki, J. Eastoe, L. Pasupulety, Langmuir 20 (2004) 11223.
[32] J. Liu, Z. Zhao, C. Xu, A. Duan, React. Kinet. Catal. Lett. 87 (2006) 107.
[33] J.J. Yu, Z. Jiang, L. Zhu, Z.P. Hao, Z.P. Xu, J. Phys. Chem. B 110 (2006) 4291.
[34] J. Liu, Z. Zhao, C. Xu, A. Duan, G. Jiang, J. Phys. Chem. C, in press.
[35] Y. Su, M.D. Amiridis, Catal. Today 96 (2004) 31.
[36] C. Sedlmair, K. Seshan, A. Jentys, J.A. Lercher, J. Catal. 214 (2003) 308.
[37] I. Nova, L. Castoldi, L. Lietti, E. Tronconi, P. Forzatti, F. Prinetto, G. Ghiotti, J. Catal. 222 (2004) 377.
[38] X. Xu, J. Li, Z. Hao, J. Rare Earths 24 (2006) 172.
[39] N. Imanaka, T. Masui, K. Minami, K. Koyabu, Chem. Mater. 17 (2005) 6511.
[40] X. Xu, C. Song, Appl. Catal. A 300 (2006) 130.
[41] R. Burch, Catal. Rev. 46 (2004) 271.
[42] K. Tikhomirov, O. Krócher, M. Elsener, A. Wokaun, Appl. Catal. B 64 (2006) 72.
[43] I. Atribak, I. Such-Basáñez, A. Bueno-López, A. García, J. Catal. 250 (2007) 75.